

University of Galway Research Repository

Towards a kinetic understanding of the NO_x promoting-effect on ignition of coalbed methane: A case study of methane/nitrogen dioxide mixtures

Title	Towards a kinetic understanding of the NO _x promoting-effect on ignition of coalbed methane: A case study of methane/nitrogen dioxide mixtures
Author(s)	Deng, Fuquan;Yang, Feiyu;Zhang, Peng;Pan, Youshun;Bugler, John;Curran, Henry J.;Zhang, Yingjia;Huang, Zuohua
Publication Date	2016-05-03
Publication information	Deng, Fuquan, Yang, Feiyu, Zhang, Peng, Pan, Youshun, Bugler, John, Curran, Henry J., Zhang, Yingjia, Huang, Zuohua. (2016). Towards a kinetic understanding of the NO _x promoting-effect on ignition of coalbed methane: A case study of methane/nitrogen dioxide mixtures. Fuel, 181, 188-198. doi: http://dx.doi.org/10.1016/j.fuel.2016.04.090
Publisher	Elsevier
Link to publisher's version	http://dx.doi.org/10.1016/j.fuel.2016.04.090
Item record	http://hdl.handle.net/10379/6263

1 **Towards a Kinetic Understanding of the NO_x Promoting-Effect on**
2 **Ignition of Coalbed Methane: A Case Study of Methane/Nitrogen**
3 **Dioxide mixtures**

4 Fuquan Deng^a, Feiyu Yang^a, Peng Zhang^a, Youshun Pan, John Bugler^b,
5 Henry J. Curran^b, Yingjia Zhang^{a,b*}, Zuohua Huang^a

6 *a. State Key Laboratory of Multiphase Flows in Power Engineering, Xi'an Jiaotong University,*
7 *Xi'an 710049, People's Republic of China*

8 *b. Combustion Chemistry Centre, National University of Ireland, Galway, Ireland.*

9 **Abstract**

10 Nitrogen dioxide (NO₂) is an important impurity in coal-bed methane (CBM) and a dominant
11 component of NO_x pollution in practical engines. Its promoting effect on methane ignition has been
12 studied in the current experimental and kinetic study. Ignition delay times of NO₂/CH₄/O₂/Ar
13 mixtures, with blending ratios of NO₂:CH₄ of 30:70, 50:50 and 70:30 for stoichiometric methane
14 mixtures were measured in a shock tube. Experiments cover a range of pressures (1.2 – 10.0 atm)
15 and temperatures (933 – 1961 K). Under all tested pressures, NO₂ addition promotes the reactivity
16 of methane and reduces the global activation energy at all pressures, and these effects are most
17 significant for the mixtures with highest NO₂ concentrations, at the highest pressures and at the
18 lowest temperatures. To simulate the experimental measurements, five literature NO_x sub-
19 mechanisms were integrated with AramcoMech 1.3. The simulations demonstrate that, for the
20 mixtures with low levels of NO_x concentrations, the five models agree well with the experimental
21 ignition delay times. For the mixtures with high NO_x content, however, all five models are unable to
22 reproduce the measured data, and the level of disagreement increases with increasing NO₂
23 concentration. An updated mechanism is proposed, based on modifications made as a result of

24 sensitivity and reaction flux analyses performed to quantitatively determine the chemical reasons
25 for NO₂ promoting methane ignition. The results indicate that, NO₂ addition perturbs the branching
26 ratio of key reaction pathways by affecting the structure of the free radical pool at the initial ignition
27 stage of methane oxidation. A new reaction cycle *via* the following sequence of reactions $\dot{\text{C}}\text{H}_3 +$
28 $\text{NO}_2 \rightleftharpoons \text{CH}_3\dot{\text{O}} + \text{NO}$, $\text{CH}_3\dot{\text{O}} + \text{M} \rightleftharpoons \text{CH}_2\text{O} + \dot{\text{H}} + \text{M}$, $\text{NO}_2 + \dot{\text{H}} \rightleftharpoons \text{NO} + \dot{\text{O}}\text{H}$, and $\text{CH}_4 + \dot{\text{O}}\text{H}$
29 $\rightleftharpoons \dot{\text{C}}\text{H}_3 + \text{H}_2\text{O}$ is proposed to explain the observed effect of NO₂ addition on the promotion of
30 methane ignition.

31
32 **Keywords:** Shock tube; CH₄; NO₂; Ignition delay time; Kinetic model

33 ***Corresponding author:**

34 Yingjia Zhang

35 Telephone: 86-29-82665075. Fax: 86-29-82668789.

36 E-mail: yjzhang_xjtu@mail.xjtu.edu.cn (Yingjia Zhang).

37

38 1. Introduction

39 Coal-bed methane (CBM), a form of natural gas extracted from coal beds, has been considered
40 as a clean alternative fuel for decades^{1, 2}, especially in coal-rich countries like America, Russia,
41 Canada, Australia and China. However, there are assignable impurity components such as nitrogen
42 oxide (NO_x), sulfur oxide (SO_x), carbon monoxide (CO) and carbon dioxide (CO₂) present in CBM
43 that can significantly influence the combustion and emission performance of internal combustion
44 engines and gas turbines³⁻⁸. For an internal combustion engine with exhaust gas recirculation, for
45 example, the NO_x formed during fuel combustion will be recirculated into the next combustion
46 cycle and will then influence the combustion phase and induce a potential engine knock by
47 promoting the reactivity of the fresh mixture in the combustion chamber^{3, 4, 9, 10}.

48 Previous studies indicate that the presence of NO_x can significantly reduce ignition delay times
49 (τ_{ign}) of methane^{6, 7, 11-16}, reflecting the importance of NO_x for the combustion of CBM/natural gas in
50 practical combustion devices. Several experimental and modeling investigations of the sensitization
51 effect of NO_x on methane ignition have been conducted. Faravelli et al.¹⁴ developed a detailed NO_x
52 mechanism to examine the impact of NO on hydrocarbon combustion at low-temperature
53 conditions. They reported that the NO significantly promotes the oxidation of hydrocarbons and this
54 observation was more obvious for large alkanes relative to alkenes and methane. Sivaramakrishnan
55 et al.¹⁶ studied the effect of NO addition to fuel-lean CH₄/C₂H₆/O₂/Ar mixtures: 1) at 50 atm in a
56 high-pressure shock tube (HPST); 2) at 10 atm and at 1000 – 1500 K in a jet stirred reactor (JSR).
57 They observed that the mixture reactivity was enhanced by the formation of abundant $\dot{\text{O}}\text{H}$ radicals
58 with NO addition *via* the reaction $\text{NO} + \text{H}\dot{\text{O}}_2 \rightleftharpoons \text{NO}_2 + \dot{\text{O}}\text{H}$. Rasmussen et al.¹³ performed an
59 investigation on the NO_x/CH₄/O₂ system using N₂ as diluent over a temperature range of 600 – 900
60 K at pressures of 20 – 100 bar in a high-pressure laminar flow reactor. They found that NO_x
61 dramatically reduced the initiation temperature, while nitromethane (CH₃NO₂) formed at elevated

62 pressures, temporarily inhibited the reactivity of the mixtures. They attributed the promoting effect
63 of NO_x on a chain-propagating NO/NO_2 cycle. Gersen et al.⁹ studied the effect of NO_2 addition on
64 ignition delay times of methane, ethane and methane/ethane mixtures in a rapid compression
65 machine (RCM) at pressures of 25 – 50 bar and at initial temperatures of 900 – 1050 K. Their
66 results indicated that NO_2 obviously reduced the reactivity of all the mixtures tested, but only
67 exhibited a limited effect on ethane ignition.

68 Recently, Herzler and Naumann⁶ investigated the promoting effect of NO_2 on methane/ethane
69 mixtures in a HPST using NO_2 concentrations of 20 – 250 ppm at pressures of approximately 16 bar
70 and equivalence ratios of 0.25 – 1.0 over a temperature range of 1000 – 1700 K. They observed a
71 similar promoting effect of NO_2 as those measured in previous studies. In addition, Herzler and
72 Naumann⁶ combined a hydrocarbon mechanism with four NO_x sub-models (Faravelli et al. model¹⁴,
73 Sivaramakrishnan et al. model¹⁶, Rasmussen et al. model¹³ and Hori et al. model⁵), and found that
74 all mechanisms predicted similar ignition delay times. More recently, Mathieu et al.⁷ explored the
75 effect of NO_2 addition to methane mixtures on ignition delay times at pressures of 1 – 28 atm and at
76 equivalence ratios of 0.5 – 2.0 with the mole fraction ratios of $\text{NO}_2:\text{CH}_4$ varying from 1.7:10 to 7:10
77 in a HPST. They indicated that the addition of NO_2 reduced ignition times of methane mixtures, and
78 the reduction was more obvious at elevated pressure. Moreover, Mathieu et al. proposed an updated
79 NO_x model and compared it with three literature ones (Gersen et al. model⁹, Sivaramakrishnan et al.
80 model¹⁶ and Mevel and Shepherd model¹⁷). Differences in the predictions of the four models were
81 observed at their investigated conditions.

82 Considering the literature review above, these previous studies have focused on mixtures with
83 relatively-low concentrations of nitrogen dioxide. There is no direct experimental evidence to
84 determine whether the available NO_x models can be applied to simulate the auto-ignition behavior
85 of mixtures with high levels of NO_x .

86 The first aim of *this paper* is to provide ignition delay times of $\text{NO}_2/\text{CH}_4/\text{O}_2/\text{Ar}$ mixtures with

87 three high blending ratios of NO₂ with NO₂:CH₄ mole fraction ratios of 30:70, 50:50 and 70:30 at
88 pressures from 1.2 to 10.0 atm and over a wide range of temperatures. The second aim is to evaluate
89 the performance of currently available NO_x sub-mechanisms assembled with AramcoMech 1.3
90 compared to our new data. Finally, an updated NO_x model will be proposed and used to conduct a
91 kinetic analysis of the NO₂ sensitizing-effect during the methane ignition process.

92 **2. Experimental**

93 All of the current experiments were performed in a stainless steel shock tube, described in a
94 previous study¹⁸⁻²⁰. Briefly, the shock tube has an internal diameter of 11.5 cm with a 4.8 m long
95 driven-section and a 4.0 m long driver-section divided by double polyethylene terephthalate (PET)
96 diaphragms. Before each experiment, the shock tube was first evacuated to around 10 Pa using a
97 mechanical vacuum pump and was subsequently vacuumed to below 1 Pa using a roots vacuum
98 pump, with a leak rate of less than 1 Pa/min. The NO₂/CH₄/O₂/Ar mixtures were prepared in
99 advance in a 128 L stainless steel tank using Dalton's law of partial pressure, and allowed to
100 homogenize for more than 12 hours to ensure sufficient mixing and diffusion. The mixing tank was
101 also evacuated to below 1 Pa before mixture preparation. The mixture components used in *this*
102 *study* were CH₄ (> 99.99%), O₂ (> 99.99%), Ar (> 99.99%) and NO₂ (up to 99.99%) diluted to 20%
103 with Ar. Different ratios of high-purity He and N₂ (in purities of up to 99.999% and 99.999%
104 respectively) were used to achieve a tailored condition so as to obtain a longer test time.

105 Four fast-response piezoelectric pressure transducers (PCB 113B26), installed in the last 1.3 m
106 of the shock tube with the same interval of 300 mm, were used to trigger three time-counters
107 (FLUKE PM6690) to record the time intervals, which were used to calculate the incident shock
108 velocities. The shock velocity was extrapolated to the end-wall to obtain the reflected-shock
109 conditions using a chemical equilibrium software GASEQ²¹.

110 It was suggested in the work of Petersen et al.²² that the uncertainty of the reflected temperature

111 was mainly attributable to the uncertainty of the incident shock velocity, which is determined by the
 112 uncertainties in the distances of the pressure transducers and shock pass time recorded by the time-
 113 counters. We have adopted a standard root-sum-squares (RSS) method used by Petersen et al.²²,

$$114 \quad T_5 = \frac{T_1 [2(\gamma-1)M^2 + (3-\gamma)] [(3\gamma-1)M^2 - 2(\gamma-1)]}{(\gamma+1)^2 M^2} = AM^2 + B + CM^{-2} \quad (1)$$

$$115 \quad M = \frac{V_s}{\sqrt{\gamma RT_1}} \quad (2)$$

$$116 \quad \delta V_s = \sqrt{\left(\frac{1}{\Delta t} \delta_{\Delta z}\right)^2 + \left(\frac{-\Delta z}{\Delta t^2} \delta_{\Delta t}\right)^2} \quad (3)$$

$$117 \quad \delta T_5 = \frac{\partial T_5}{\partial M} \delta M = (2AM - 2CM^{-3}) \frac{\delta V_s}{\sqrt{\gamma RT_1}} \quad (4)$$

118 where T_5 is the reflected shock temperature (K); T_1 is the initial temperature (K); γ is the adiabatic
 119 exponent; V_s is the velocity of the incident shock wave (m/s); and R is the universal gas constant.
 120 The uncertainty of the time measured by the FLUKE PM6690 time-counter was estimated to be
 121 1000 ns, which is equal to the sum total of random and systematic uncertainties for the FLUKE
 122 PM6690 counter timer and resolution time for the pressure transducers. The uncertainty in distance
 123 between the pressure transducers was estimated to be $2 \times 1000 \text{ ns} \times V_s$, which stems mainly from
 124 the diameter of the sensing area of the pressure transducers and the shock front thickness. Using Eqs.
 125 1 – 4, the largest uncertainty in the reflected temperature is estimated to be 20 K. However, this
 126 uncertainty of the reflected shock temperature leads to a 20% uncertainty in measured ignition
 127 times, τ_{ign} , based on an Arrhenius type correlation of τ_{ign} using the RSS method, a detailed
 128 description of which can be found in our previous study²³.

129 The reflected-shock pressure was detected using a piezoelectric pressure transducer with
 130 acceleration compensation (PCB 113B03) located in the endwall. A photomultiplier
 131 (HAMAMASSU CR131), installed in the endwall, was used to record OH* light emission through a
 132 307 nm narrowband (5 nm) filter. The measured pressure and OH* profiles at the endwall were used

133 to determine the ignition event. The ignition delay time is defined as the time interval between the
134 arrival of the incident shock wave at the endwall and the extrapolation of the maximum slope of
135 OH* emission to the baseline, Fig. 1. Note that an obvious pressure rise ($dp/dt = 4\%/ms$) can be
136 observed before the main ignition due to an interaction between the reflected shock wave and the
137 boundary layer as motioned in our previous study¹⁸, and this has been included in our numerical
138 simulations.

139 To confirm the reliability of the current facility, a confirmatory experiment was conducted for a
140 NO₂/CH₄/O₂/Ar mixture at an identical condition to that already published in the literature⁷. Figure
141 2 shows a comparison between the ignition delay times measured in *this study* and those measured
142 by Mathieu et al. data for the mixture with 70.8% NO₂ addition at $\varphi = 0.5$ and $p = 1.3$ atm. Overall,
143 the current data agrees well with the literature data, by considering both ignition delay times and
144 global activation energy.

145 3. Kinetic model evaluation

146 All of the simulation and kinetic analysis for CH₄/NO₂ mixtures were carried out using the
147 CHEMKIN²⁴ program with the SENKIN²⁵ code. As mentioned above, the rate of pressure rise
148 ($dp/dt = 4.0\%/ms$) was considered in the simulations using the SENKIN/VTIM approach as
149 proposed in the literature²⁶. The simulated ignition delay time is defined as the time of maximum
150 dT/dt , as this is very similar to the experimental definition.

151 AramcoMech 1.3²⁷, developed at NUI Galway in 2013, which was selected as the base model
152 for methane oxidation, has been systematically modified and validated against a wide range of
153 experimental targets including shock tube ignition delay times, RCM ignition delay times, laminar
154 flame speed, JSR species mole fraction, and flow reactor speciation. Figure 3 shows a comparison
155 between the experiments and the predictions using AramcoMech 1.3 for mixtures with no NO₂
156 added (N₀), in the temperature range 1400 – 2050 K and at pressures of 1.2 – 10.0 atm. It appears

157 that AramcoMech 1.3 agrees reasonably well with the measured results under all experimental
158 conditions.

159 Regarding the NO_x chemistry, five literature models were chosen, namely those from
160 Sivaramakrishnan et al.¹⁶, Rasmussen et al.²⁸, Mathieu et al.⁷, Gersen et al.⁹ and Faravelli et al.¹⁵,
161 with all models containing detailed NO_x sub-models. Specifically, Rasmussen's NO_x sub-model
162 includes 62 species and 501 reactions and was developed based on their studies of NO_x effects on
163 methane¹³, ethylene²⁸ and syngas²⁹. This model has been validated against a large set of data
164 obtained in flow reactor, JSR, RCM, shock tube and laminar flames. Gersen's NO_x sub-model,
165 containing 61 species and 479 reactions, is based on the work of Rasmussen et al.²⁸, with some
166 amendments: 1) the rate constants of the reactions $\text{CH}_4 + \text{NO}_2 = \dot{\text{C}}\text{H}_3 + \text{HONO}$ and $\text{CH}_4 + \text{NO}_2 =$
167 $\dot{\text{C}}\text{H}_3 + \text{HNO}_2$ were replaced by the evaluations of Dean and Bozzelli³⁰; 2) the rate constants of the
168 reactions $\text{C}_2\text{H}_6 + \text{NO}_2$ and $\text{C}_2\text{H}_4 + \text{NO}_2$ were taken by an analogy with the reaction of CH₄ with
169 NO₂. Sivaramakrishnan's NO_x sub-model includes 38 species and 278 reactions, and has been
170 validated against data from HPST, JSR and flow reactor. Mathieu's⁷ NO_x sub-model includes 36
171 species and 305 reactions. The NH₃/NO_x chemistry was taken from Dagaut et al.³¹, with the H₂/N₂O
172 chemistry being adopted from Mathieu et al.³² and the hydrocarbon/NO_x interactions chemistry was
173 taken from Sivaramakrishnan et al.¹⁶. Faravelli's¹⁵ NO_x sub-model contains 30 species and 260
174 reactions. This model has also been validated against experimental data from shock tube, JSR and
175 laminar flame.

176 To better compare the NO_x sub-models, the five literature NO_x sub-models mentioned above
177 were combined with AramcoMech 1.3 in order to minimize the effect of the hydrocarbon sub-
178 mechanism. Herein, the five combined models are called Aramco-S, Aramco-R, Aramco-M,
179 Aramco-G and Aramco-F model, respectively. Figures 4–6 show the comparisons between the
180 measured ignition delay times and the model predictions using the five assembled models. The
181 results indicate that the five models exhibit only slightly different predictions of ignition delay times

182 for mixtures with relatively low NO₂ content, Fig. 4, but there is an obvious difference in the
183 predictions of these models and this discrepancy becomes more significant with increasing
184 concentrations of NO₂, Figs 5 and 6. Previously, Herzler and Naumann⁶ performed a similar study,
185 i.e. they combined different NO_x sub-mechanisms (Rasmussen et al.²⁸, Faravelli et al.¹⁵ and
186 Sivaramakrishnan et al.¹⁶) to a hydrocarbon sub-mechanism and then simulated the reactivity of
187 NO_x/hydrocarbon mixtures. They found that the different NO_x sub-mechanisms only presented a
188 negligible difference. This observation from Herzler and Naumann⁶ is only consistent with that for
189 the N₃₀ mixture in *this study* while it is inconsistent for the N₅₀ and N₇₀ mixtures. Obviously, the
190 different results are mainly attributable to the different NO₂ concentrations used. It can be therefore
191 inferred that all of the recent NO_x models can give good predictions for mixtures with low
192 concentrations of NO₂, but they cannot accurately predict the reactivity for mixtures with high NO₂
193 concentrations.

194 For the N₃₀ mixture, Fig. 4, the predictions of all five models agree with the measured ignition
195 delay times at $T < 1280$ K but under-predict the experimental data at $T > 1280$ K in the pressure
196 range of 1.2 – 10.0 atm, and the discrepancies are more obvious with increasing pressures. For the
197 N₅₀ mixture, Fig. 5, the five models under-predict the ignition delay times at 1.2 and 4.0 atm at all
198 temperatures tested. When the pressure increases to 10.0 atm, the Aramco-F, Aramco-M and
199 Aramco-S models show an acceptable agreement with the measured data at $T < 1200$ K, but still
200 under-predict at $T > 1200$ K. For the N₇₀ mixture, Fig. 6, the Aramco-G, Aramco-F and Aramco-R
201 models moderately agree with the experimental results at $T < 1175$ K but become much faster at $T >$
202 1175 K, while the Aramco-M and Aramco-S models agree moderately at $T > 1175$ K but over-
203 predict the experimental ignition delay times at $T < 1175$ K.

204 As discussed above, the Aramco-M model exhibits generally better agreement compared to the
205 experimental data although it shows an under-prediction at high-temperatures for the N₃₀ and N₅₀
206 mixtures and an over-prediction of the ignition delay times at low-temperatures for the N₇₀ mixture.

207 Thus, the Aramco-M model was selected as the base model to develop a more accurate mechanism
208 for methane/NO_x mixtures.

209 Firstly, the C₂-hydrocarbon/NO_x interaction chemistry in the Aramco-M model was updated
210 using recently published C₂-hydrocarbon/NO_x subsets from Gersen et al.⁹. Thereafter, the rate
211 constants of several key reactions, which were recognized through sensitivity analyses, were updated
212 to obtain better simulation agreement against our experimental data. All of the changes/additions to
213 the Aramco-M model are shown in Table 1. The thermochemistry of NO_x related species has been
214 re-calculated at NUI Galway with three quantum-chemical compound methods (CBS-APNO, G3
215 and G4) and the B3LYP/cc-pVTZ level of theory³³, and these new data have been adopted in our
216 updated mechanism. Figure 7 shows the performance of the modified mechanism against the
217 experimental data. It appears that the updated model captures well both the global activation energy
218 and ignition delay times for all of the mixtures tested over the range of physical conditions.
219 Additionally, the updated model has been used to simulate the ignition delay times reported by
220 Mathieu et al.⁷ and Herzler and Naumann⁶, and the comparisons are provided in the *Supplementary*
221 *Material*. Generally, the model exhibits good agreement compared to the literature data.

222 4. Results and discussion

223 In *this study*, the ignition delay times were measured behind the reflected shock waves for four
224 stoichiometric NO₂/CH₄/O₂/Ar mixtures with different NO₂ concentrations (N₀, N₃₀, N₅₀ and N₇₀) at
225 1.2, 4.0 and 10.0 atm. Here NO₂ was only regarded as a part of the argon used as diluent gas. The
226 detailed compositions of the tested mixtures are shown in Table 2 and all experimental data are
227 provided in the *Supplemental Material*.

228 4.1 Pressure-dependence of CH₄/NO₂ mixtures

229 As with most hydrocarbons, the trends with respect to the influence of pressure on the ignition

230 delay times are in-line for all tested mixtures, Fig. 7. Moreover, the pressure effect increases with
231 increasing the NO₂ blending ratio. Particularly, the reductions in τ_{ign} are a factor of 2.43, 2.36, 2.63
232 and 3.08 (high-temperature) and 1.98, 2.01, 2.12 and 2.35 (low-temperature) for the N₀, N₃₀, N₅₀
233 and N₇₀ mixtures, respectively, when the pressure is changed from 1.2 to 10.0 atm. Clearly, the
234 reduction in τ_{ign} with an increase in pressure for the N₃₀ mixture is less obvious than the pure
235 methane one but is the reverse of the trend observed for the N₅₀ and N₇₀ mixtures. Mathieu et al.⁷
236 reported that the reduction in ignition delay times with increasing pressure for NO₂/CH₄ mixtures
237 was less important than for pure methane mixtures. The different observations can be attributed to
238 the different NO₂ concentrations present in the mixtures. In the Mathieu et al. study, the
239 concentration of NO₂ is similar to that of the N₃₀ mixture in *this study*, and there is therefore a
240 similar pressure-dependence with methane, Fig. 7a. However, with increasing NO₂ addition as in
241 the N₅₀ and N₇₀ mixtures, the pressure-dependence of the mixtures is notably affected by the
242 CH₄/NO₂ chemistry, meaning that the reactivity of mixtures containing higher concentrations of
243 NO₂ is more sensitive to a change in pressure compared to methane, Figs. 7b and 7c.

244 4.2 The effect of NO₂ on methane reactivity

245 Figure 8 illustrates the effects of NO₂ addition on methane ignition at pressures of 1.2, 4.0 and
246 10.0 atm. It is seen that the presence of NO₂ significantly reduces τ_{ign} of methane over the entire
247 temperature range. Moreover, the reduction in τ_{ign} increases with increasing NO₂ concentrations.
248 Similar observations have also been found in previous studies of the NO₂ sensitization effect on
249 hydrocarbons^{6, 7}. Note that this reduction in τ_{ign} is lessened at elevated pressures, which is also
250 observed by Mathieu et al.⁷. In addition, the reduction in τ_{ign} presents a considerable temperature-
251 dependence. Specifically, at 1.2 atm, Fig. 8a, the N₃₀, N₅₀, and N₇₀ mixtures exhibit a 78.5%, 89.0%
252 and 94.1% reduction in τ_{ign} at low-temperatures. At 4.0 atm, Fig. 8b, an 83.8%, 93.5% and 97.5%
253 reduction can be observed for the N₃₀, N₅₀ and N₇₀ mixtures at low-temperatures. However, at 10.0

254 atm, Fig. 8c, the results shows a reduction of up to 86.1%, 95.1% and 98.3% for the N₃₀, N₅₀ and
255 N₇₀ mixtures at low-temperatures.

256 For a given mixture, the dependence of ignition delay times on temperature follows a simple
257 Arrhenius behavior, and the correlations are proposed based on the study of Davidson et al.³⁴, as
258 shown in the following format:

$$259 \quad \tau = Ap^n \exp(E_a / RT) \quad (5)$$

260 Where τ is the ignition delay time (μs), p is the pressure (atm), T is the temperature (K) and E_a is the
261 global activation energy ($\text{kcal} \cdot \text{K}^{-1} \text{mol}^{-1}$), R is the universal gas constant (equal to 1.9872×10^{-3}
262 $\text{kcal K}^{-1} \text{mol}^{-1}$). The correlations obtained are as follows:

263 N₀:

$$264 \quad \tau = -5.7 p^{-0.64} \exp(42.15 / RT) \quad (6)$$

265 N₃₀ ($T > 1350$ K):

$$266 \quad \tau = -2.18 p^{-0.56} \exp(26.13 / RT) \quad (7)$$

267 N₅₀:

$$268 \quad \tau = -2.0 p^{-0.69} \exp(24.11 / RT) \quad (8)$$

269 N₇₀:

$$270 \quad \tau = -2.4 p^{-0.72} \exp(22.41 / RT) \quad (9)$$

271 It is observed that the exponent of pressure for the N₃₀ mixture is smaller to that of the N₀
272 mixture indicating that ignition delay times are less sensitive to a change in pressure for the N₃₀
273 mixture. For the N₅₀ and N₇₀ mixtures however, the exponents of pressure are greater than that for
274 the N₀ mixture, indicating that ignition delay times are more sensitive to a change in pressure for
275 high NO₂ concentrations. Moreover, the results show an obvious reduction in the global activation
276 energy with increasing NO₂ concentration, with this reduction becoming moderate with increasing
277 NO₂ concentration.

278 5. Kinetic analysis

279 5.1 Sensitivity analysis

280 To identify the key reactions in the CH₄/NO₂ system, a brute force sensitivity analysis to
281 ignition delay time was conducted for the four mixtures tested in *this study* at 1500 K and 4.0 atm
282 using the modified Aramco-M model. Here, a sensitivity coefficient is defined as a perturbation
283 caused by a change in A-factor for each reaction rate constant³⁵ as follows:

$$284 \quad S_i = \frac{\tau(2k_i) - \tau(0.5k_i)}{1.5\tau(k_i)} \quad (10)$$

285 where τ is the ignition delay time of the combustible mixture, k_i is rate constant of the i^{th} reaction
286 and S_i is sensitivity coefficient of i^{th} reaction. A negative value means that the reaction promotes
287 reactivity and vice versa.

288 The most-sensitive reactions of the pure methane and CH₄/NO₂ mixtures at 4.0 atm and 1500 K
289 are displayed in Figs. 9 and 10, respectively. For the N₀ mixture, Fig. 9, the chain-branching
290 reaction R1 ($\dot{\text{H}} + \text{O}_2 \rightleftharpoons \ddot{\text{O}} + \dot{\text{O}}\text{H}$) shows the biggest negative sensitivity coefficient, while the
291 parallel reactions R148 ($\dot{\text{C}}\text{H}_3 + \text{O}_2 \rightleftharpoons \text{CH}_3\dot{\text{O}} + \ddot{\text{O}}$) and R149 ($\dot{\text{C}}\text{H}_3 + \text{O}_2 \rightleftharpoons \text{CH}_2\text{O} + \dot{\text{O}}\text{H}$) present
292 relatively-high negative sensitivity coefficients as a two-fold effect: a) the consumption of an
293 unreactive methyl radical can form highly reactive free $\ddot{\text{O}}$ atoms or $\dot{\text{O}}\text{H}$ radicals which promote
294 reactivity; b) the $\text{CH}_3\dot{\text{O}}$ radical can directly decompose to form another $\dot{\text{H}}$ atom *via* $\text{CH}_3\dot{\text{O}} + \text{M} \rightleftharpoons$
295 $\text{CH}_2\text{O} + \dot{\text{H}} + \text{M}$. Reaction 129 ($\text{CH}_4 + \dot{\text{H}} \rightleftharpoons \dot{\text{C}}\text{H}_3 + \text{H}_2$) exhibits the highest positive sensitivity
296 coefficient as a highly reactivity $\dot{\text{H}}$ atom is consumed to form a relatively unreactive $\dot{\text{C}}\text{H}_3$ radical. It
297 appears that the most sensitive reactions associated with the ignition of pure methane involve $\dot{\text{C}}\text{H}_3$
298 radicals, indicating that the production and consumption of these are critical in controlling methane
299 ignition. Compared to larger hydrocarbons, in methane oxidation these fuel radicals do not readily
300 react with O₂ *via* R148 and R149 to form further free radicals due to lower conversion rates of $\dot{\text{C}}\text{H}_3$
301 radicals. It is well known that fuel radicals reacting with O₂ is typically one of the global rate

302 limiting steps during low-temperature hydrocarbon combustion. Therefore, as mentioned in
303 previous studies^{36,37}, the two reactions above are responsible for the longer ignition delay times of
304 methane oxidation compared to other hydrocarbons.

305 Unlike pure methane, several of the newly-added reactions exhibit a high sensitivity coefficient
306 for the mixtures with NO₂ added to methane, Fig. 10. This means that NO₂ addition is responsible
307 for a significant perturbation in the radical pool generated during methane oxidation. Methyl
308 radicals can be preferentially oxidized by NO₂ *via* R1017 ($\dot{\text{C}}\text{H}_3 + \text{NO}_2 \rightleftharpoons \text{CH}_3\dot{\text{O}} + \text{NO}$) in the
309 mixtures containing NO₂ rather than by O₂ *via* R148 and R149 for the pure methane mixture,
310 leading to R1017 becoming the second-most important reaction in terms of increasing reactivity and
311 reducing the importance of R148 and R149. This reduction increases with an increase in NO₂
312 concentration. Figure 11 shows a comparison of the rate constants for R1017, R148 and R149. It
313 appears that the rate constant of R1017 is greater than that of R148 and R149 by orders of
314 magnitude. As a result, the consumption of $\dot{\text{C}}\text{H}_3$ radicals is dramatically promoted *via* R1017,
315 leading to an increased concentration of $\dot{\text{H}}$ atoms through the decomposition of CH₃ $\dot{\text{O}}$ radicals.
316 Furthermore, R952 ($\text{NO}_2 + \dot{\text{H}} \rightleftharpoons \text{NO} + \dot{\text{O}}\text{H}$) is the most inhibiting reaction due to its competition
317 for $\dot{\text{H}}$ atoms with R1. Note that methane preferentially undergoes H-atom abstraction by $\dot{\text{O}}\text{H}$
318 radicals rather than by $\dot{\text{H}}$ atoms in the presence of NO₂, causing the dramatic decreases in the
319 sensitivity of R129 and the obvious increase in sensitivity of R130 ($\text{CH}_4 + \dot{\text{O}}\text{H} \rightleftharpoons \dot{\text{C}}\text{H}_3 + \text{H}_2\text{O}$).

320 For the mixtures containing a high concentration of NO₂, N₅₀ and N₇₀, methane is almost
321 completely consumed *via* H-atom abstraction by $\dot{\text{O}}\text{H}$ radicals. An obvious reduction in the
322 sensitivity coefficients of R129 and R190 ($\dot{\text{C}}\text{H}_3 + \dot{\text{C}}\text{H}_3 (+ \text{M}) \rightleftharpoons \text{C}_2\text{H}_6 (+ \text{M})$) with NO₂ addition is
323 observed as less methane is consumed *via* R130 and fewer $\dot{\text{C}}\text{H}_3$ radicals react *via* R190.
324 Particularly, the sensitivity coefficient of R1 increases for the N₃₀ mixture but decreases with
325 increasing NO₂ concentration. The initial added NO₂ is mainly consumed through R952, and a
326 small amount reacts through R1017. For the N₃₀ mixture, the initial added NO₂ is quickly consumed

327 completely *via* R952 and R1017, and the production of $\dot{\text{H}}$ atoms and $\dot{\text{O}}\text{H}$ radicals in the presence of
328 NO_2 enhances reaction R1. For the N_{50} and N_{70} mixtures, however, the high initial NO_2
329 concentration persists for a long time before ignition, so R952 competes with R1 for $\dot{\text{H}}$ atoms, and a
330 reduction in sensitivity coefficient of R1 can be seen with increasing NO_2 concentration.

331 5.2 Kinetic effect of NO_2 addition on reaction pathway of methane

332 To further understand the chemical interaction between NO_2 and CH_4 , a reaction pathway/flux
333 analysis was performed using the updated Aramco-M model at 4.0 atm and 1500 K, and at 20%
334 CH_4 consumption. For the pure methane mixture, the fuel molecules are largely consumed *via* H-
335 atom abstraction reactions by $\dot{\text{H}}$ and $\dot{\text{O}}$ atoms and $\dot{\text{O}}\text{H}$ radicals to form $\dot{\text{C}}\text{H}_3$ radicals, Fig. 12.
336 Subsequently, $\dot{\text{C}}\text{H}_3$ radicals are consumed *via* three reaction pathways: the first (56.8%) in which
337 $\dot{\text{C}}\text{H}_3$ radicals undergo a radical-radical self-recombination termination reaction to generate ethane,
338 inhibiting reactivity; the second (12.5%) in which $\dot{\text{C}}\text{H}_3$ radicals react with O_2 to form formaldehyde
339 and $\dot{\text{O}}\text{H}$ radicals *via* a chain propagation reaction which actually promotes reactivity; the third
340 (6.3%) in which $\dot{\text{C}}\text{H}_3$ radicals react with HO_2 radicals in a chain branching reaction to produce $\dot{\text{O}}\text{H}$
341 and $\text{CH}_3\dot{\text{O}}$ radicals which readily decompose to formaldehyde and $\dot{\text{H}}$ atoms. Note that in the
342 presence of NO_2 , almost all of the methane fuel (84.5%, 95.1 and 96.3% for the N_{30} , N_{50} and N_{70}
343 mixtures, respectively) is consumed *via* H-atom abstraction by $\dot{\text{O}}\text{H}$ radicals. In addition, with
344 increasing NO_2 addition, the consumption of the $\dot{\text{C}}\text{H}_3$ radicals *via* the self-recombination reaction
345 reduces to 13.8%, 2.4% and $< 1.0\%$ for the N_{30} , N_{50} and N_{70} mixtures, respectively. It can
346 significantly drive the ignition because less $\dot{\text{C}}\text{H}_3$ radicals are transformed into stable C_2H_6
347 molecules *via* the chain termination of R190. This means that more $\dot{\text{C}}\text{H}_3$ radicals, 63.2%, 84.4% and
348 89.1%, are oxidized by NO_2 to form $\text{CH}_3\dot{\text{O}}$ radicals *via* R1017. As a result, more $\dot{\text{H}}$ atoms are
349 generated from $\text{CH}_3\dot{\text{O}}$ radical decomposition with increasing concentrations of NO_2 and thus will
350 accelerate fuel consumption *via* H-atom abstraction.

351 5.3 Rate of production analysis with NO₂ addition

352 As described above, the production of $\dot{\text{O}}\text{H}$ radicals is critical to the promoting effect of NO₂ on
353 methane ignition. Here, the mole fractions of $\dot{\text{O}}\text{H}$ radicals produced as a function NO₂ addition at
354 4.0 atm and 1500 K are plotted in Fig. 13. It appears that the peak in $\dot{\text{O}}\text{H}$ mole fraction is
355 comparable for the four mixtures tested near the main ignition. However, the $\dot{\text{O}}\text{H}$ radical mole
356 fraction obviously increases with increasing NO₂ concentration during the induction time. It means
357 that there is a chemical environment to rapidly consume methane before the main ignition. To
358 demonstrate the simulated observation, rates of production of CH₄ and $\dot{\text{O}}\text{H}$ radicals were carried out
359 under the same condition, Fig. 14. The results indicate that reaction R1 largely contributes to the
360 production of $\dot{\text{O}}\text{H}$ radicals, while reactions R3 ($\dot{\text{O}}\text{H} + \text{H}_2 \rightleftharpoons \dot{\text{H}} + \text{H}_2\text{O}$) and R27 ($\text{CO} + \dot{\text{O}}\text{H} \rightleftharpoons$
361 $\text{CO}_2 + \dot{\text{H}}$) mainly consume $\dot{\text{O}}\text{H}$ radicals for the mixture without NO₂. For all of the key reactions
362 presented in Fig. 14a, the contributed rate peaks are displayed in the position nearby the main
363 ignition. However, the rates of consumption and production of $\dot{\text{O}}\text{H}$ radicals *via* reactions R1, R3 and
364 R27 decrease with increasing NO₂ addition, while the development of $\dot{\text{O}}\text{H}$ radicals *via* reaction
365 R130 consuming $\dot{\text{O}}\text{H}$ radicals and reaction R952 producing $\dot{\text{O}}\text{H}$ radicals is observed to be more
366 important. Particularly, for the N₇₀ mixture, reactions R952 and R130 displace R1, R3 and R27 in
367 becoming the most important $\dot{\text{O}}\text{H}$ radical production and consumption reactions, respectively. It is
368 worth noting that the peaks contributed by R952 and R130 in the rate of production analysis appear
369 during the induction time rather than at the main ignition. This indicates that the free radical pool
370 will be pre-established at the initial stage of ignition by NO₂ addition, leading to methane can be
371 consumed *via* R130 at the ignition induced time. This confirms the simulation result observed in
372 Fig. 13. In fact, methane is largely consumed by H-atom abstraction by $\dot{\text{H}}$ and $\ddot{\text{O}}$ atoms and $\dot{\text{O}}\text{H}$
373 radicals and *via* R129, R131 ($\text{CH}_4 + \ddot{\text{O}} \rightleftharpoons \dot{\text{C}}\text{H}_3 + \dot{\text{O}}\text{H}$) and R130, for the mixtures with low NO₂
374 content. However, for the mixtures with high NO₂ content, namely the N₅₀ and N₇₀ mixtures, only
375 R130 is observed to be competitive in consuming methane, Fig. 14b. There is a clearly different

376 oxidation cycle pathway from pure methane in the presence of NO₂, namely, the $\dot{\text{C}}\text{H}_3$ radicals
377 formed by R130 goes to feed R1017 to produce more CH₃ $\dot{\text{O}}$ radicals which readily decompose to
378 generate reactive $\dot{\text{H}}$ atoms and promote the formation of $\dot{\text{O}}\text{H}$ radicals *via* R952. The abundant $\dot{\text{O}}\text{H}$
379 radicals formed from R952 further accelerate the methane oxidation *via* R130. This also explains
380 why R130 becomes the important reaction promoting reactivity in Fig. 9 for high concentrations of
381 NO₂ present in the CH₄/NO₂ mixtures.

382 **6. Conclusions**

383 Ignition delay times of NO₂/CH₄/O₂/Ar mixtures with mole blending ratio of NO₂:CH₄ = 0,
384 30:70, 50:50 and 70:30 were measured behind reflected shock waves at pressures ranging from 1.2
385 to 10.0 atm and for temperatures ranging from 933 to 1961 K. A kinetic analysis was performed
386 using a modified model to interpret the promoting effect of NO₂ on methane ignition. The main
387 conclusions are summarized as follows,

- 388 1) The addition of NO₂ significantly reduces ignition delay times of methane oxidation. The
389 reduction is more prominent with decreasing temperature and increasing pressure. The
390 promoting effect of NO₂ is more remarkable for the mixtures with higher NO₂
391 concentration. Moreover, the addition of NO₂ reduces the global activation energy of
392 methane and the reduction becomes more moderate with increasing NO₂ addition.
- 393 2) Five assembled models (Aramco-M, Aramco-G, Aramco-R, Aramco-S and Aramco-F) were
394 used to simulate the measured ignition delay times. For the mixtures with low NO₂
395 concentrations, (N₀ and N₃₀) the five models present similar predictions and agree with the
396 experimental data. However, the five models do not predict well the experimental
397 measurements for the mixtures with higher NO₂ content (N₅₀ and N₇₀).
- 398 3) An updated model is proposed to simulate the current data and other literature data and has
399 been used to conduct a kinetic analysis. NO₂ addition benefits the free radical pool

400 especially $\dot{\text{O}}\text{H}$ radical formation in the initial ignition stage of methane, and perturbs the
401 branching ratios of key reactions. Compared to pure methane, the formation of $\dot{\text{O}}\text{H}$ radicals
402 occurs mainly *via* the inter-conversion of NO_2 and NO *via* R952 ($\text{NO}_2 + \dot{\text{H}} \rightleftharpoons \text{NO} + \dot{\text{O}}\text{H}$)
403 rather than R1 ($\dot{\text{H}} + \text{O}_2 \rightleftharpoons \ddot{\text{O}} + \dot{\text{O}}\text{H}$), while more stable $\dot{\text{C}}\text{H}_3$ radicals prefer to undergo
404 reaction R1017 ($\dot{\text{C}}\text{H}_3 + \text{NO}_2 \rightleftharpoons \text{CH}_3\dot{\text{O}} + \text{NO}$) in a chain-propagation process rather than
405 radical self-recombination *via* R190 ($\dot{\text{C}}\text{H}_3 + \dot{\text{C}}\text{H}_3 (+ \text{M}) \rightleftharpoons \text{C}_2\text{H}_6 (+ \text{M})$).

406 **Acknowledgements**

407 The authors would like to acknowledge funding under the National Natural Science Foundation of
408 China (No. 51206132, 91441203) and National Basic Research Program (2013CB228406). The
409 authors also appreciate the funding support of Fundamental Research Funds for the Central
410 Universities.

411

412 **References**

- 413 1. Tian, L.; Cao, Y.; Chai, X.; Liu, T.; Feng, P.; Feng, H.; Zhou, D.; Shi, B.; Oestreich, R.;
414 Rodvelt, G. Best practices for the determination of low-pressure/permeability coalbed methane
415 reservoirs, Yuwu Coal Mine, Luan mining area, China. *Fuel* **2015**, 160, 100-107.
- 416 2. Rightmire, C. Coalbed methane resource. **1984**.
- 417 3. Nicolle, A.; Dagaut, P. Occurrence of NO-reburning in MILD combustion evidenced via
418 chemical kinetic modeling. *Fuel* **2006**, 85 (17), 2469-2478.
- 419 4. Dubreuil, A.; Foucher, F.; Mounai, C.; Dayma, G.; Dagaut, P. HCCI combustion: Effect of NO
420 in EGR. *Proc. Combust. Inst.* **2007**, 31 (2), 2879-2886.
- 421 5. Hori, M.; Matsunaga, N.; Marinov, N.; William, P.; Charles, W. In *An experimental and kinetic*
422 *calculation of the promotion effect of hydrocarbons on the NO-NO₂ conversion in a flow reactor*,
423 Symposium (International) on Combustion, **1998**; Elsevier: 1998; pp 389-396.
- 424 6. Herzler, J.; Naumann, C. Shock Tube Study of the Influence of NO_x on the Ignition Delay
425 Times of Natural Gas at High Pressure. *Combust. Sci. Technol.* **2012**, 184 (10-11), 1635-1650.
- 426 7. Mathieu, O.; Pemelton, J. M.; Bourque, G.; Petersen, E. L. Shock-induced ignition of methane
427 sensitized by NO₂ and N₂O. *Combustion and Flame* **2015**.
- 428 8. Dayma, G.; Dagaut, P. Effects of air contamination on the combustion of hydrogen—effect of
429 NO and NO₂ addition on hydrogen ignition and oxidation kinetics. *Combust. Sci. Technol.* **2006**,
430 178 (10-11), 1999-2024.
- 431 9. Gersen, S.; Mokhov, A.; Darneveil, J.; Levinsky, H.; Glarborg, P. Ignition-promoting effect of
432 NO₂ on methane, ethane and methane/ethane mixtures in a rapid compression machine. *Proc.*
433 *Combust. Inst.* **2011**, 33 (1), 433-440.
- 434 10. Chong, J.; Tsolakis, A.; Gill, S.; Theinnoi, K.; Golunski, S. E. Enhancing the NO₂/NO_x ratio in
435 compression ignition engines by hydrogen and reformat combustion, for improved aftertreatment

436 performance. *Int. J. Hydrogen Energy* **2010**, 35 (16), 8723-8732.

437 11. Dabora, E. Effect of NO₂ on the ignition delay of CH₄-air mixtures. *Combust. Flame* **1975**, 24,
438 181-184.

439 12. Konnov, A. Implementation of the NCN pathway of prompt-NO formation in the detailed
440 reaction mechanism. *Combust. Flame* **2009**, 156 (11), 2093-2105.

441 13. Rasmussen, C. L.; Rasmussen, A. E.; Glarborg, P. Sensitizing effects of NO_x on CH₄ oxidation
442 at high pressure. *Combust. Flame* **2008**, 154 (3), 529-545.

443 14. Faravelli, T.; Frassoldati, A.; Ranzi, E. Kinetic modeling of the interactions between NO and
444 hydrocarbons in the oxidation of hydrocarbons at low temperatures. *Combust. Flame* **2003**, 132 (1),
445 188-207.

446 15. Frassoldati, A.; Faravelli, T.; Ranzi, E. Kinetic modeling of the interactions between NO and
447 hydrocarbons at high temperature. *Combust. Flame* **2003**, 135 (1), 97-112.

448 16. Sivaramakrishnan, R.; Brezinsky, K.; Dayma, G.; Dagaut, P. High pressure effects on the
449 mutual sensitization of the oxidation of NO and CH₄-C₂H₆ blends. *Phys. Chem. Chem. Phys.* **2007**,
450 9 (31), 4230-4244.

451 17. Mével, R.; Shepherd, J. Ignition delay-time behind reflected shock waves of small
452 hydrocarbons-nitrous oxide (-oxygen) mixtures. *Shock Waves* **2015**, 25 (3), 217-229.

453 18. Zhang, Y.; Huang, Z.; Wei, L.; Zhang, J.; Law, C. K. Experimental and modeling study on
454 ignition delays of lean mixtures of methane, hydrogen, oxygen, and argon at elevated pressures.
455 *Combust. Flame* **2012**, 159 (3), 918-931.

456 19. Zhang, Y.; Huang, Z.; Wei, L.; Niu, S. Experimental and kinetic study on ignition delay times
457 of methane/hydrogen/oxygen/nitrogen mixtures by shock tube. *Chinese Sci. Bull.* **2011**, 56 (26),
458 2853-2861.

459 20. Zhang, J.; Pan, L.; Zhang, Z.; Mo, J.; Huang, Z. Shock tube and kinetic modeling study of
460 isobutanal oxidation. *Energy Fuels* **2013**, 27 (5), 2804-2810.

- 461 21. Morley, C. Gaseq: a chemical equilibrium program for Windows. [http:// www. gaseq. co. uk](http://www.gaseq.co.uk)
462 **2005**.
- 463 22. Petersen, E. L.; Rickard, M. J.; Crofton, M. W.; Abbey, E. D.; Traum, M. J.; Kalitan, D. M. A
464 facility for gas-and condensed-phase measurements behind shock waves. *Measurement Sci.*
465 *Technol.* **2005**, 16 (9), 1716.
- 466 23. Zhang, Z.; Hu, E.; Pan, L.; Chen, Y.; Gong, J.; Huang, Z. Shock-Tube Measurements and
467 Kinetic Modeling Study of Methyl Propanoate Ignition. *Energy Fuels* **2014**, 28 (11), 7194-7202.
- 468 24. Kee, R. J.; Rupley, F. M.; Miller, J. A. *Chemkin-II: A Fortran chemical kinetics package for the*
469 *analysis of gas-phase chemical kinetics*; Sandia National Labs., Livermore, CA (USA): **1989**.
- 470 25. Lutz, A. E.; Kee, R. J.; Miller, J. A. *SENKIN: A fortran program for predicting homogeneous*
471 *gas phase chemical kinetics with sensitivity analysis*; Sandia National Labs., Livermore, CA (USA):
472 1988.
- 473 26. Chaos, M.; Dryer, F. L. Chemical - kinetic modeling of ignition delay: Considerations in
474 interpreting shock tube data. *Int. J. Chem. Kinet.* **2010**, 42 (3), 143-150.
- 475 27. Metcalfe, W. K.; Burke, S. M.; Ahmed, S. S.; Curran, H. J. A hierarchical and comparative
476 kinetic modeling study of C₁- C₂ hydrocarbon and oxygenated fuels. *Int.l J. Chem. Kinet.* **2013**, 45
477 (10), 638-675.
- 478 28. Lopez, J. G.; Rasmussen, C. L.; Alzueta, M. U.; Gao, Y.; Marshall, P.; Glarborg, P.
479 Experimental and kinetic modeling study of C₂H₄ oxidation at high pressure. *Proc. Combust. Inst.*
480 **2009**, 32 (1), 367-375.
- 481 29. Rasmussen, C. L.; Hansen, J.; Marshall, P.; Glarborg, P. Experimental measurements and
482 kinetic modeling of CO/H₂/O₂/NO_x conversion at high pressure. *Int. J. Chem. Kinet.* **2008**, 40 (8),
483 454-480.
- 484 30. Dean, A. M.; Bozzelli, J. W. Combustion chemistry of nitrogen. In *Gas-phase combustion*
485 *chemistry*, Springer: **2000**; pp 125-341.

- 486 31. Dagaut, P.; Glarborg, P.; Alzueta, M. U. The oxidation of hydrogen cyanide and related
487 chemistry. *Prog. Energy Combust. Sci.* **2008**, 34 (1), 1-46.
- 488 32. Mathieu, O.; Levacque, A.; Petersen, E. Effects of N₂O addition on the ignition of H₂-O₂
489 mixtures: Experimental and detailed kinetic modeling study. *Int. J. Hydrogen Energy* **2012**, 37 (20),
490 15393-15405.
- 491 33. Bugler, J.; Somers, K. P.; Simmie, J. M.; Guthe, F.; Curran, H. J. *Proc. Combust. Inst.* **2015**,
492 submitted.
- 493 34. Davidson, D.; Oehlschlaeger, M.; Herbon, J.; Hanson, R. Shock tube measurements of iso-
494 octane ignition times and OH concentration time histories. *Proc. Combust. Inst.* **2002**, 29 (1), 1295-
495 1301.
- 496 35. Zhang, J.; Wei, L.; Man, X.; Jiang, X.; Zhang, Y.; Hu, E.; Huang, Z. Experimental and
497 modeling study of n-butanol oxidation at high temperature. *Energy Fuels* **2012**, 26 (6), 3368-3380.
- 498 36. Takita, K.; Abe, N.; Masuya, G.; Ju, Y. Ignition enhancement by addition of NO and NO₂ from
499 a N₂/O₂ plasma torch in a supersonic flow. *Proc. Combust. Inst.* **2007**, 31 (2), 2489-2496.
- 500 37. Chen, Z.; Qin, X.; Ju, Y.; Zhao, Z.; Chaos, M.; Dryer, F. L. High temperature ignition and
501 combustion enhancement by dimethyl ether addition to methane-air mixtures. *Proc. Combust. Inst.*
502 **2007**, 31 (1), 1215-1222.
- 503
- 504
- 505
- 506

507

508 **Table 1.** List of updated reactions rate constants.

Reactions	Reaction rate constant			Reference
	A	n	E_a	
$\text{CH}_3+\text{NO}_2 \rightleftharpoons \text{CH}_3\text{O}+\text{NO}$	1.28E+13	-0.2	0.0	[16]
$\text{CH}_2\text{O}+\text{NO}_2 \rightleftharpoons \text{HCO}+\text{HONO}$	1.40E-07	5.640	9220.0	[28]
$\text{NO}_3+\text{NO}_2 \rightleftharpoons \text{NO}_2+\text{NO}+\text{O}_2$	2.35E+10	0.000	2960.0	[16]
$\text{HONO}+\text{OH} \rightleftharpoons \text{NO}_2+\text{H}_2\text{O}$	1.70E+12	0.000	-520.0	[16]
$\text{NO}_2+\text{O} \rightleftharpoons \text{NO}+\text{O}_2$	1.00E+14	-0.520	0.000	[9]

509 Units = $\text{cm}^3 \text{mole}^{-1} \text{s}^{-1} \text{cal}^{-1}$.

510

511 **Table 2.** The compositions of mixtures measured in the present experiment.

Mixture	Mole blending ratio	CH_4	NO_2	O_2	AR
N_0	100% CH_4	0.0190	0.0000	0.0381	0.9429
N_{30}	30% NO_2 /70% CH_4	0.0190	0.0081	0.0384	0.9345
N_{50}	50% NO_2 /50% CH_4	0.0187	0.0187	0.0371	0.9255
N_{70}	70% NO_2 /30% CH_4	0.0189	0.0435	0.0379	0.8997

512

513 **Figures captions**

514 **Fig.1.** Typical measured pressure and OH^* profiles at the end-wall for N_{30} mixture at 4.0 atm and
515 1315 K.

516 **Fig.2.** Comparison between the measured data and the predictions using Aramco 1.3 for N_0 at
517 different pressures.

518 **Fig.3.** Comparison between the measured data and the predictions with five assembled models for
519 N_{30} mixture at different pressures. (a) 1.2 atm, (b) 4.0 atm, (c) 10.0 atm.

520 **Fig.4.** Comparison between the measured data and the predictions with five assembled models for
521 N_{50} mixture at different pressure. (a) 1.2 atm, (b) 4.0 atm, (c) 10.0 atm.

522 **Fig.5.** Comparison between the measured data and the predictions with five assembled models for
523 N_{70} mixture at different pressures. (a) 1.2 atm, (b) 4.0 atm, (c) 10.0 atm.

524 **Fig.6.** Comparison between the measured ignition delay times and the model predictions with
525 updated model for the CH_4/NO_2 mixtures. (a) N_{30} , (b) N_{50} , (c) N_{70} .

526 **Fig.7.** Comparison of the current and literature data for CH_4/NO_2 with 70.8% blend ratio at 1.3 atm
527 and $\phi = 0.5$.

528 **Fig.8.** Effect of NO_2 blending ratio on the ignition delay time of methane at pressure from 1.2 to
529 10.0 atm. Symbols: experiments; Lines: simulations with updated model. (a) 1.2 atm; (b) 4.0 atm;
530 (c) 10.0 atm.

531 **Fig.9.** Normalized sensitivity analysis for neat CH_4 at $p = 4.0$ atm and $T = 1500$ K using updated
532 model.

533 **Fig.10.** Normalized sensitivity analysis for N_{30} , N_{50} and N_{70} at $p = 4.0$ atm and $T = 1500$ K using
534 updated model. The normalized sensitivity coefficient of R1: $\dot{H} + O_2 \rightleftharpoons \ddot{O} + \dot{O}H$ is divided by 2.

535 **Fig.11.** Comparison of the rate constants for the reactions R148, R149 and R1017.

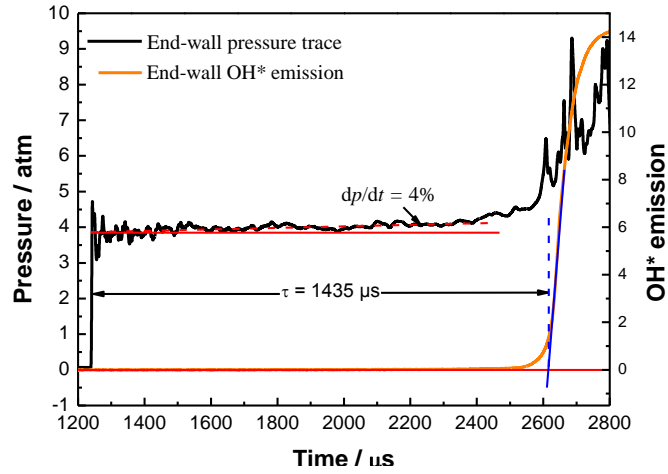
536 **Fig.12.** Reaction pathway analysis of four mixtures at 4 atm and 1500 K using updated model. N_0 :
537 black, N_{30} : red, N_{50} : blue, and N_{70} : green.

538 **Fig.13.** Mole fraction of $\dot{O}H$ growth during ignition of CH_4/NO_2 mixtures at $p = 4.0$ atm and $T =$
539 1500 K using updated model.

540 **Fig.14.** Rate of productions for $\dot{O}H$ and CH_4 in CH_4/NO_2 ignition process at $p = 4.0$ atm and $T =$
541 1500 K using updated model. (a) rate of $\dot{O}H$ production analysis; (b) rate of CH_4 production
542 analysis.

543

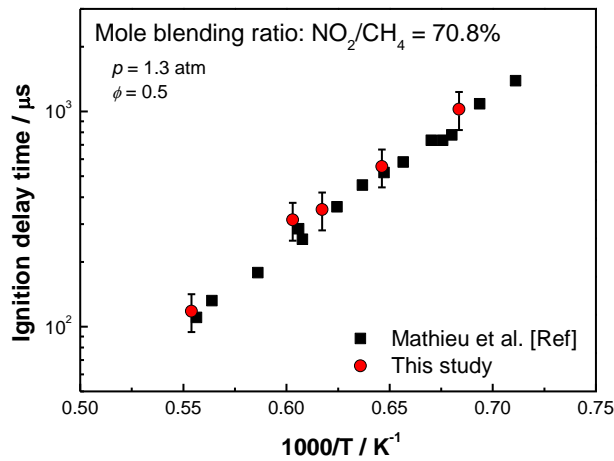
544



545

546 **Fig.1.** Typical measured pressure and OH* profiles at the end-wall for N₃₀ mixture at 4.0 atm and

547 1315 K.



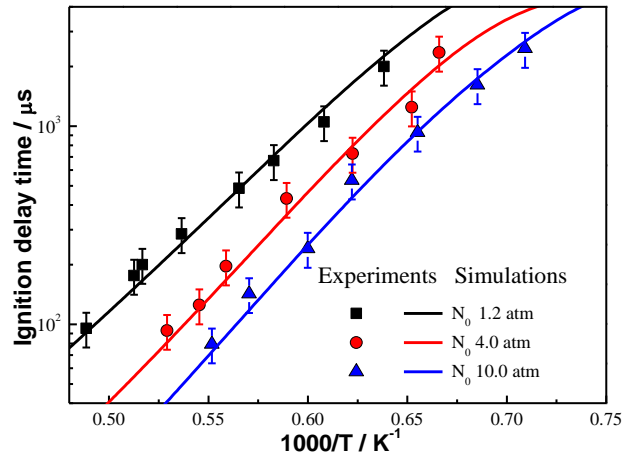
548

549 **Fig.2.** Comparison of the current and literature data for CH₄/NO₂ with 70.8% blend ratio at 1.3 atm

550 and $\phi = 0.5$.

551

552

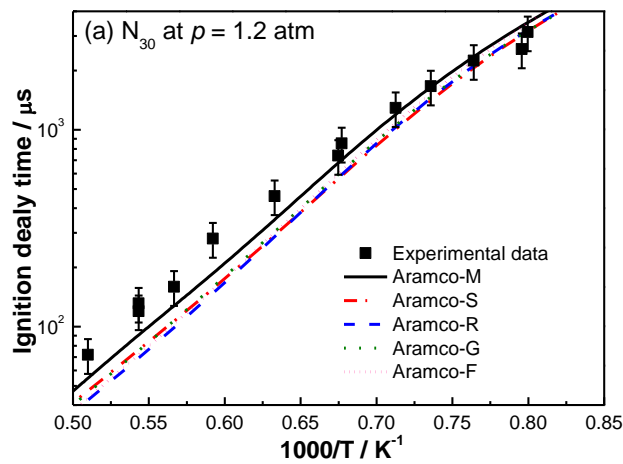


553

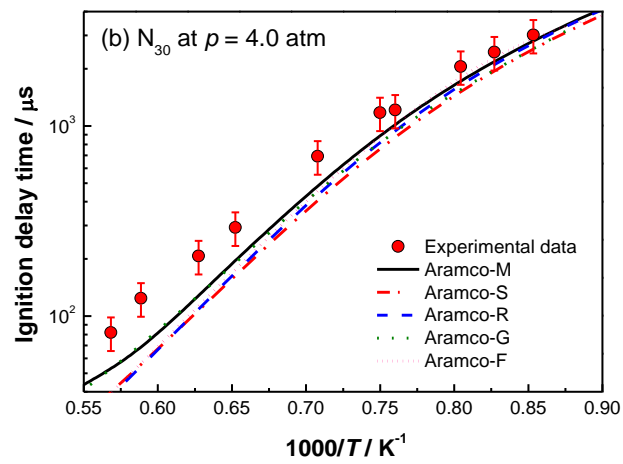
554 **Fig.3.** Comparison between the measured data and the predictions using AramcoMech 1.3 for N_0 at

555 different pressures.

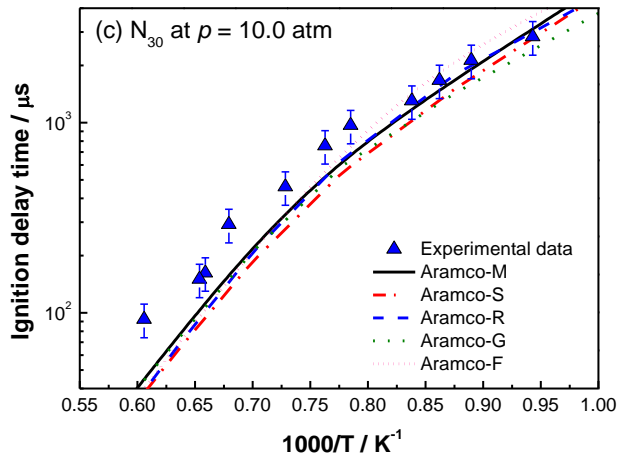
556



557



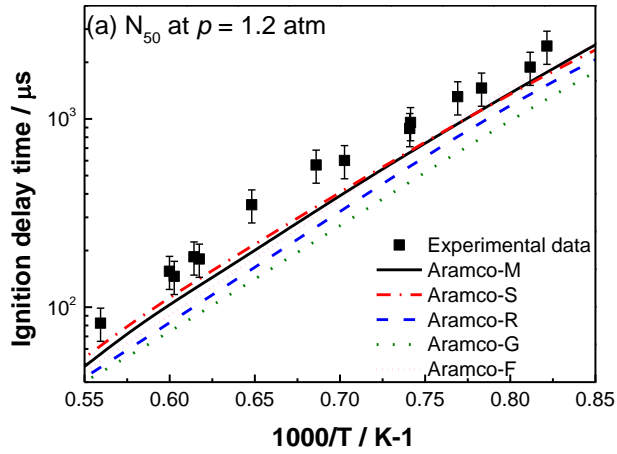
558



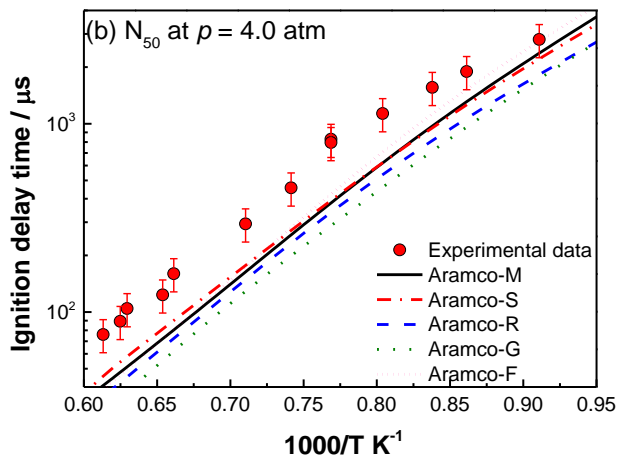
559

560 **Fig.4.** Comparison between the measured data and the predictions with five assembled models for
 561 N_{30} mixture at different pressures. (a) 1.2 atm, (b) 4.0 atm, (c) 10.0 atm.

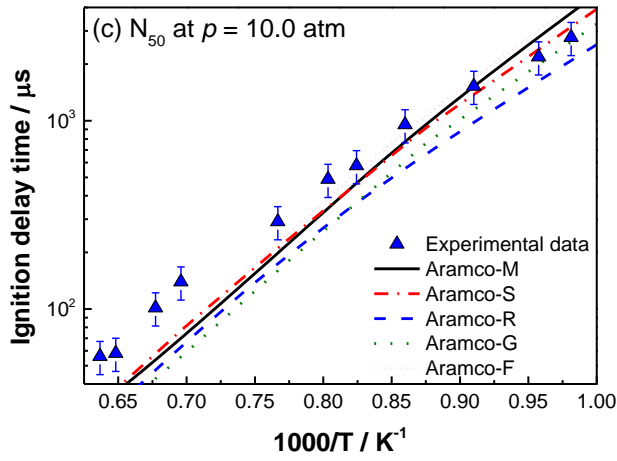
562



563



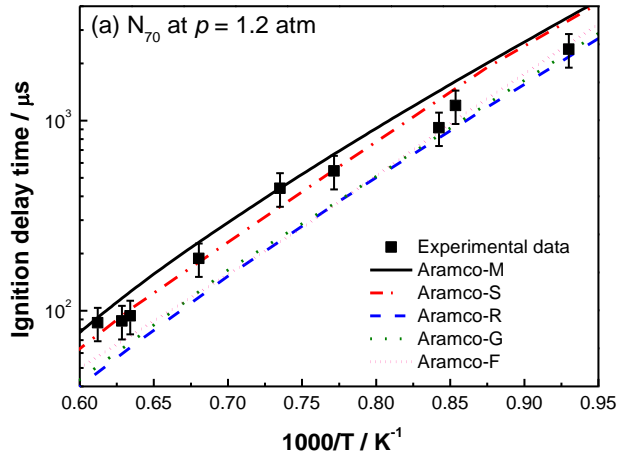
564



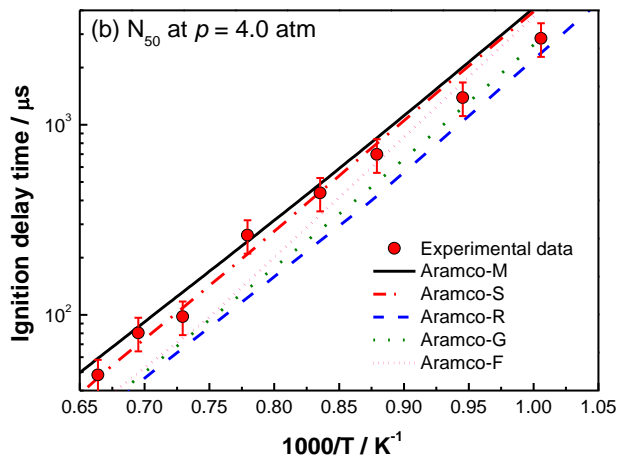
565

566 **Fig.5.** Comparison between the measured data and the predictions with five assembled models for
 567 N_{50} mixture at different pressure. (a) 1.2 atm, (b) 4.0 atm, (c) 10.0 atm.

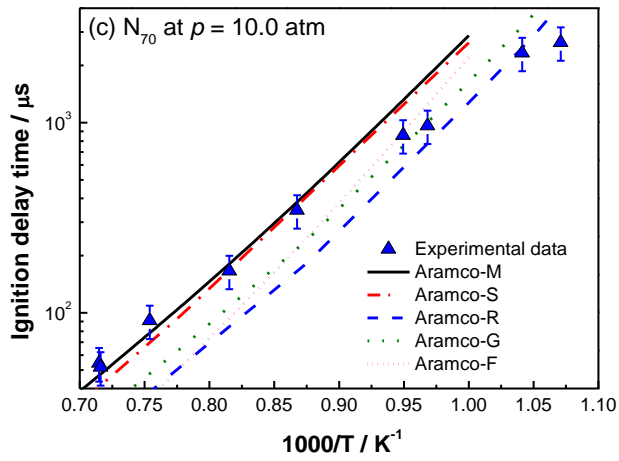
568



569



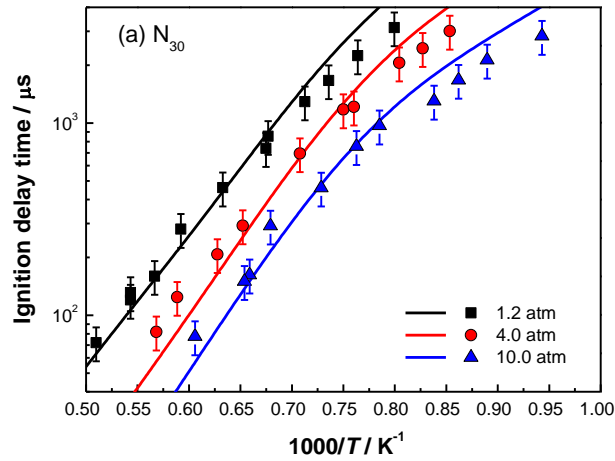
570



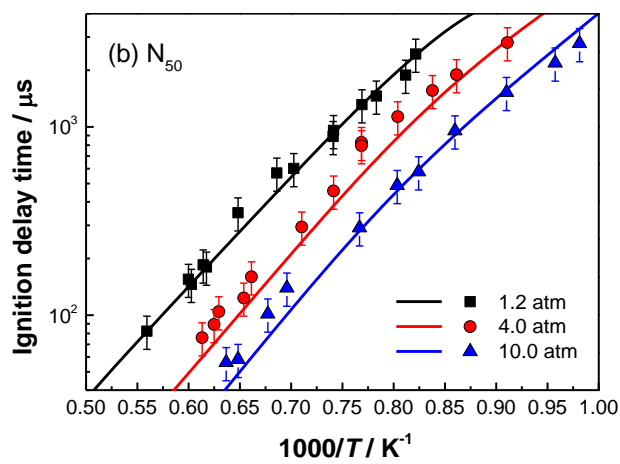
571

572 **Fig.6.** Comparison between the measured data and the predictions with five assembled models for
 573 N_{70} mixture at different pressures. (a) 1.2 atm, (b) 4.0 atm, (c) 10.0 atm.

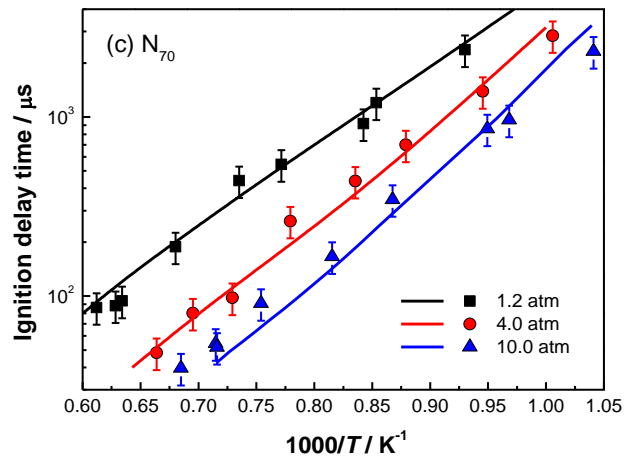
574



575



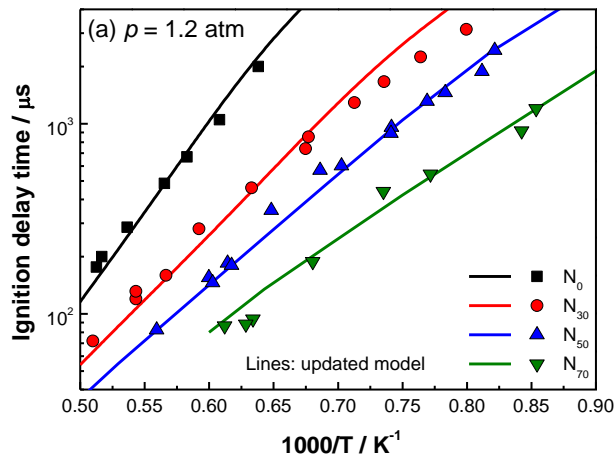
576



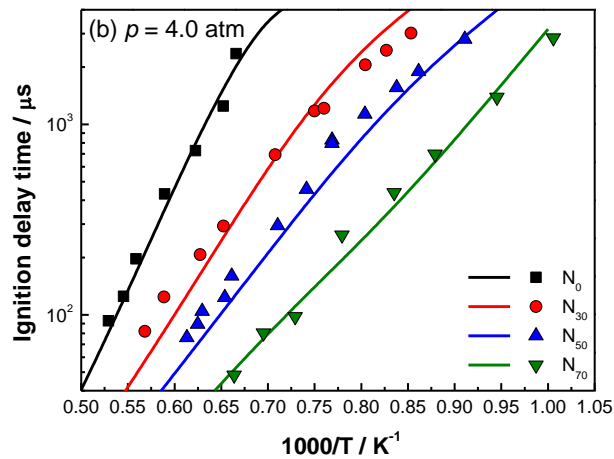
577

578 **Fig.7.** Comparison between the measured ignition delay times and the model predictions with
 579 updated model for the CH₄/NO₂ mixtures. (a) N₃₀, (b) N₅₀, (c) N₇₀.

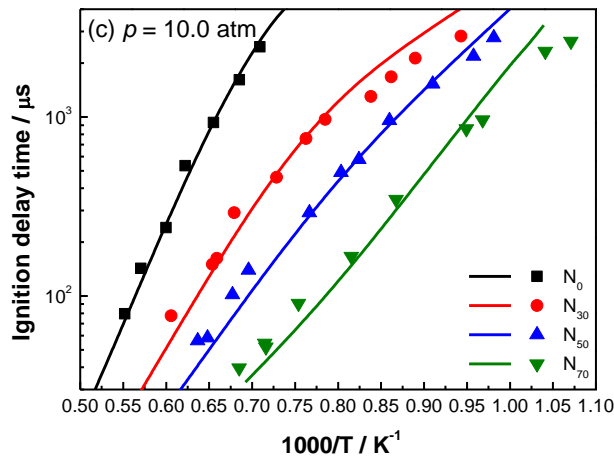
580



581



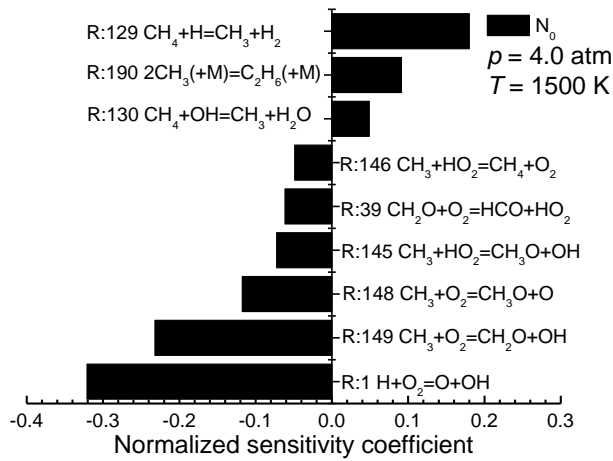
582



583

584 **Fig.8.** Effect of NO₂ blending ratio on the ignition delay time of methane at pressure from 1.2 to
 585 10.0 atm. Symbols: experiments; Lines: simulations with updated model. (a) 1.2 atm; (b) 4.0 atm; (c)
 586 10.0 atm.

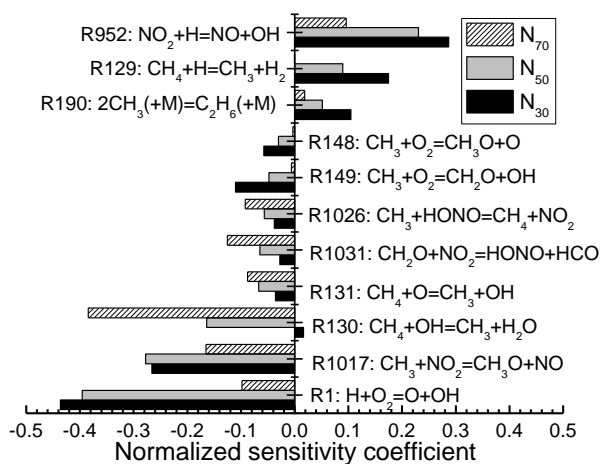
587



588

589 **Fig.9.** Normalized sensitivity analysis for neat CH₄ at $p = 4.0$ atm and $T = 1500$ K using updated
 590 model.

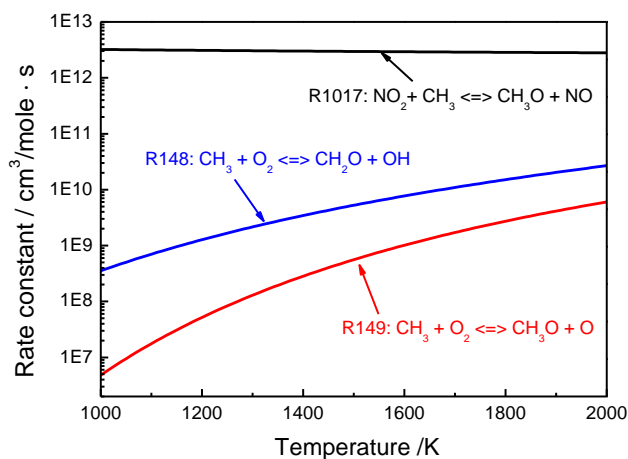
591



592

593 **Fig.10.** Normalized sensitivity analysis for N₃₀, N₅₀ and N₇₀ at $p = 4.0$ atm and $T = 1500$ K using
 594 updated model. The normalized sensitivity coefficient of R1: $\dot{H} + O_2 \rightleftharpoons \dot{O} + \dot{O}H$ is divided by 2.

595

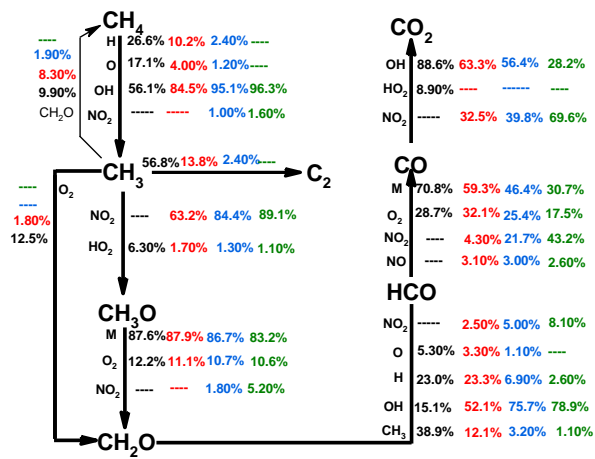


596

597 **Fig.11.** Comparison of the rate constants for the reactions R148, R149 and R1017.

598

599

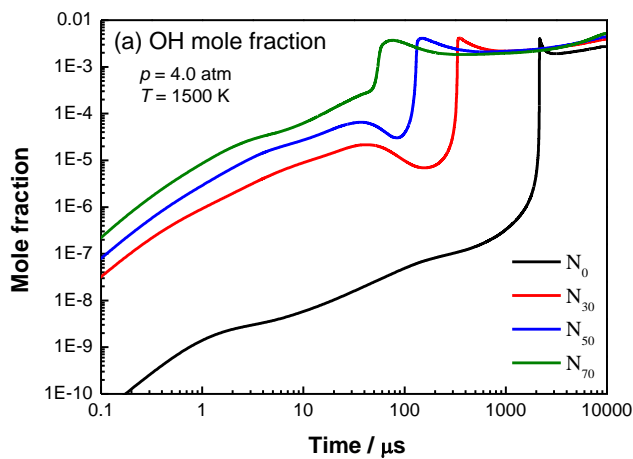


600

601 **Fig.12.** Reaction pathway analysis of four mixtures at 4 atm and 1500 K using updated model. N₀:

602 black, N₃₀: red, N₅₀: blue, and N₇₀: green.

603



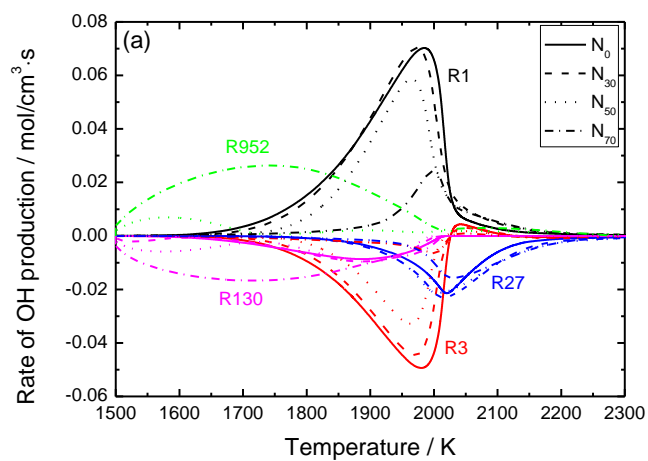
604

605 **Fig.13.** Mole fraction of $\dot{\text{O}}\text{H}$ growth during ignition of CH_4/NO_2 mixtures at $p = 4.0 \text{ atm}$ and $T =$

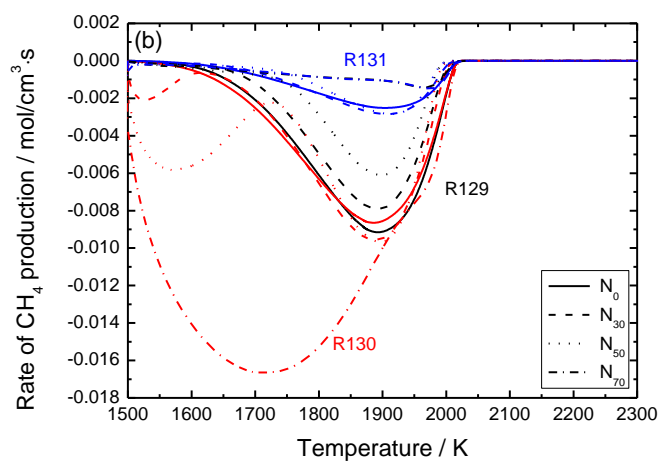
606 1500 K using updated model.

607

608



609



610 **Fig.14.** Rate of productions for $\dot{\text{O}}\text{H}$ and CH_4 in CH_4/NO_2 ignition process at $p = 4.0$ atm and $T =$
611 1500 K using updated model. (a) rate of $\dot{\text{O}}\text{H}$ production analysis; (b) rate of CH_4 production
612 analysis.

613